J Therm Spray Tech (2023) 32:1780–1795
https://doi.org/10.1007/s11666-023-01598-y

PEER REVIEWED

Influence of Ductility on Fracture in Tensile Testing of Cold Gas Sprayed Deposits

A. List[1] · C. Huang[1] · L. Wiehler[1] · C.-P. Gieseler[1] · M. Schulze[1] · F. Gärtner[1] · T. Klassen[1]

Submitted: 28 October 2022 / in revised form: 27 February 2023 / Accepted: 16 April 2023 / Published online: 17 May 2023

Abstract Cold gas spraying nowadays receives much interest for additive manufacturing due to its high deposition rate. Associated structural applications define high requirements regarding mechanical properties and failure tolerances. Up to present, micro-flat tensile (MFT) or tubular coating tensile (TCT) tests are well-established for determining deposit strengths. Due to particular stress states during testing, both provide slightly different information. While MFT tests can provide information on strain and ductility, stress concentration in TCT tests requires to apply a notch factor for calculating the ultimate tensile strength. Here, we suggest that a suitable combination of both tests can provide additional information about tolerances against local stress concentrations in crack initiation and growth. Taking titanium and copper as model systems, results from MFT and TCT tests are evaluated over a wide range of spray parameter sets into regimes that allow for high deposit qualities, even reaching certain ductility. The correlation between the results reveals that the derived stress concentration sensitivity depends on the deposit quality and could eventually decrease to unity. In turn, the correlation to respective strain to failure data can supply information on underlying deformation mechanisms. These preliminary results thus provide strategies for tuning deposit toughness and give prerequisites for quality forecasts.

Keywords additive manufacturing · cold spraying · layer ductility · mechanical properties · tensile testing

Introduction

So far, cold gas spraying (CS) has proven to be an effective technique for producing high-quality metallic coatings in many applications. More recent attention focusses on perspective application as solid-state additive manufacturing (AM) process or repair technique for structural components (Ref 1, 2). However, so far, the mechanical strength and ductility of cold sprayed deposits in an as-sprayed state often do not reach the thresholds for automotive or aerospace applications. Deeper understanding of deposit optimization is required in view of process resilience and quality control (Ref 3, 4, 5). The observed differences with respect to bulk material properties are due to some typical microstructural features obtained in cold gas spraying (Ref 6, 7). Firstly, non-bonded internal interfaces between the spray splats in the deposit could act as microcracks facilitating crack initiation and growth and ultimately fracture, resulting in limited ultimate tensile strengths (Ref 8). Secondly, the high degree of deformation during solid-state impact results in locally highly work-hardened deposit material, which does not allow for further plastic

This article is an invited paper selected from presentations at the 2022 International Thermal Spray Conference, held May 4–6, 2022, in Vienna, Austria, and has been expanded from the original presentation. The issue was organized by André McDonald, University of Alberta (Lead Editor); Yuk-Chiu Lau, General Electric Power; Fardad Azarmi, North Dakota State University; Filofteia-Laura Toma, Fraunhofer Institute for Material and Beam Technology; Heli Koivuluoto, Tampere University; Jan Cizek, Institute of Plasma Physics, Czech Academy of Sciences; Emine Bakan, Forschungszentrum Jülich GmbH; Šárka Houdková, University of West Bohemia; and Hua Li, Ningbo Institute of Materials Technology and Engineering, CAS.

✉ A. List
list@hsu-hh.de

[1] Institute of Materials Technology, Helmut Schmidt University, University of the Federal Armed Forces, Hamburg, Germany

deformation, thus locally limiting the deposit ductility and toughness (Ref 4). Therefore, cold sprayed deposits can show mechanical properties similar to highly deformed bulk material, i.e., high flow stress and, respectively, low strain to failure. The combination of both microstructural features, microcracks of different sizes and a limited toughness in their surrounding could facilitate crack nucleation and growth, and thus part failure. In consequence, to avoid both, thermal post-treatments are often applied to improve the quality of cold sprayed deposits and to meet requested property profiles. Nevertheless, to some extent, post-treatments can be avoided by well-optimized spray parameter sets that allow for some ductility and failure tolerance in as-deposited state. Respective trends for optimization can be indicated by suitable testing procedures, as derived in this paper.

In cold gas spraying, the amount of bonded internal interfaces between spray splats, and thus deposit properties are determined by the high stain rate severe plastic deformation and locally occurring adiabatic shear instabilities (ASI). Thresholds for reaching ASI are met, if the particle impact velocity (v_{imp}) exceeds the so-called critical velocity (v_{crit}) (Ref 9, 10, 11).

For a certain material, v_{crit} can be calculated for one corresponding particle impact temperature (T_{imp}) according to Eq 1 by considering the measured feedstock powder strength UTS_p, the density ρ, the heat capacity c_p, a reference temperature T_r and the melting temperature T_m (Ref 9, 12):

$$v_{\mathrm{crit}} = \sqrt{\frac{F_1 \cdot 4 \cdot UTS_p}{\rho} \cdot \left(1 - \frac{T_{\mathrm{imp}} - T_{\mathrm{ref}}}{T_m - T_{\mathrm{ref}}}\right) + F_2 \cdot c_p \cdot \left(T_m - T_{\mathrm{imp}}\right)} \quad \text{(Eq 1)}$$

Reaching conditions for ASI is here considered as prerequite for material jetting and thus bonding. Various studies have shown that ASI play a very prominent role for bonding (Ref 13, 14) and that the ASI criterion enables for a realistic predictions of critical velocities of metals, and thus attainable deposit properties (Ref 15, 16). In contrast, alternative explanations have been reported in the literature to describe the formation of material jets and bonding. Hassani-Gangaraj et al., formulate the critical velocity as a function of the bulk speed of sound (Ref 17, 18), not necessitating the formation of ASI for successful cohesive bonding (Ref 17, 18). This and other models have been controversially discussed in the literature (Ref 19). It may be noted here that the bulk speed of sound and respective fast elastic waves running through the material are determined by Young's modulus. The Young's modulus in turn is determined by chemical bonding and is only to minor extent influenced by microstructural features like grain sizes, work hardening, or even precipitates. In consequence, following the argumentation of Hassani-Gangaraj et al., recrystallization of the feedstock powders should not have a significant influence on successful bonding. However, this is clearly in contrast to works of Huang et al. (Ref 14) or Krebs et al. (Ref 21). Their feedstock powder was produced by atomization and thus had experienced quenching, and they annealed it in order to restore dislocation mobility and plasticity. These studies proved that lower powder strengths by annealing significantly reduced critical velocities for bonding, despite similar Young's modulus. These studies therefore support the model of Assadi et al., describing bonding in terms of ASI formation.

For considering the influence of the different sets of spraying parameters and particle sizes on the particle impact conditions, the so far established quality parameter η at individual impact temperatures can be calculated based on the real powder strength data (Ref 10, 14, 20, 21). This dimensionless parameter describes the ratio between v_{imp} and v_{crit}, as given in Eq 2. Impact velocities and temperatures are gained by fluid dynamics calculations and consider the particular set of process parameters and powder data.

$$\eta = \frac{v_{\mathrm{imp}}}{v_{\mathrm{crit}}} \quad \text{(Eq 2)}$$

According to Assadi et al., an η of about 1.5 is necessary to achieve good deposit quality in terms of strength, while low η values close to unity result in low deposition efficiencies and limited deposit performance (Ref 12).

Under ideal conditions, as met by shooting single bullets onto a metal surface (Ref 9), η will decide whether a particle bonds. Critical velocity and thus η being a threshold, bonding or adhesion should not occur if $\eta < 1.0$. However, the feedstock powder for cold spraying has a particular size distribution. In addition, the velocity profile of the accelerating gas in the nozzle will depend on the axial position, i.e., velocity ultimately has to go down to zero at the nozzle walls. Both will result in a statistical distribution of impact velocities and impact temperatures (Ref 22, 23). Furthermore, smaller particles may have experienced harsher quenching conditions in atomization and may thus be less ductile than larger ones, with an influence on actual critical velocity. All of this will lead to a statistical distribution around the η value, as calculated for an average particle size and assumed homogeneous bulk properties. Consequently, a certain fraction of particles will also bond and form a deposit with measurable strength even at (the average) $\eta < 1.0$. Statistics are typically reflected by a steep increase in deposition efficiency around $\eta = 1.0$, with longer tailing. Anyway, despite all uncertainties, η is serving a valuable tool to rationalize dependencies in CS.

In general, calculated velocity ratios η are needed for systematic comparison of different influences on deposit properties. With respect to structural applications, it is of high interest, whether η can also provide information on deposit failure tolerance.

For tackling this question, the major focus in the present study was put onto analyses of ultimate tensile strengths (UTS) via micro-flat tensile (MFT) as well as tubular coating tensile (TCT) tests. The combination of both is aimed to provide insights into the influence of ductility on deposit fracture behavior and local material toughness.

MFT tests were performed in accordance with DIN EN ISO 6892–1 to gain direct information about the mechanical deposit properties under uniaxial stress state (Ref 6, 24, 25). The one-dimensional stress distribution by using dog-bone-shaped flat test specimen in principle allows for deriving information on yield strength (YS), ultimate tensile strength (UTS) and elongation to failure (A*), similar to standard tensile tests (Ref 16). In contrast, the geometry of TCT tests according to DIN EN 17393 with two joined cylinders as substrates for a common, load bearing deposit just allows to derive information about UTS. In addition, the special geometry also involves multiaxial stress states in the deposit close to the cylinder face sites of the joined samples. For usually brittle samples, this stress concentration can be considered by using a fixed notch factor (NF) of about 1.6 for comparing UTS results from TCT analyses to real deposit strengths measured by MFT tests (Ref 24, 26, 27).

$$\mathrm{NF} = \frac{R_{m,\mathrm{MFT}}}{R_{m,\mathrm{TCT}}} \qquad \text{(Eq 3)}$$

With that, the stress states in given TCT test geometries show some similarity to pre-notched uniaxial tensile test samples. Thus, a systematic investigation of the correlation factor may provide information on deposit ductility and fracture toughness. For ductile systems, the stress concentration in pre-notched samples could be reduced by rounding off of originally sharp crack tips. For providing first ideas on such a concept, the present work evaluates respective influences for cold sprayed titanium (Ti) and copper (Cu) deposits, here serving as model systems.

For cold sprayed Ti deposits, it was already shown that raising the process gas temperatures from 600 to 1000 °C increases the deposit strength from 180 to 450 MPa, similar to bulk properties. However, even for highest parameter settings, the deposit ductility remained still low, indicating that non-bonded interfaces and highly work-hardened areas in the vicinity of the interfaces cannot be eliminated (Ref 27). In contrast, optimized parameter sets in cold gas spraying of Cu could result in certain deposit ductility (Ref 24, 28, 29). Recent studies report an UTS and a strain to failure of 286 MPa and 24%, respectively, by using nitrogen as process gas (750 °C and 5 MPa (Ref 28)). Experiments with He resulted in an UTS of 271 MPa and a strain to failure of 43.5% (800 °C and 2 MPa (Ref 29)). Nevertheless, so far, no correlation between MFT and TCT test results are reported that consider regimes of possible deposit ductility and thus information on consequences by stress concentrations.

This work aims to provide new insights into the strength and ductility evolution of cold sprayed deposits by parameterizing the influence of process parameter sets and testing procedures on final deformation features. For this purpose, individual spray experiments were carried out with pure Ti and pure Cu powder by using nitrogen as process gas under wide gas temperature regimes ranging from 700 up to 1000 °C for the case of Ti and from 400 up to 700 °C for Cu, respectively. Combining correlations between results from different tensile test set-ups with descriptions of impact conditions in terms of η values may improve understanding of crack growth in cold sprayed deposits. Respective concepts could then facilitate better control and prediction of deposit quality in cold spray additive manufacturing.

Materials and Methods

Feedstock Powders and Analyses

For the cold spray experiments, gas-atomized, spherical titanium grade 1 powder by AP&C (Boisbriand, Canada) and gas-atomized, spherical copper powder by Safina (Vestec, Czech Republic) were used as feedstock, respectively. The powder size distributions were determined by laser scattering, using an instrument of type LA-910 from Horiba (Kyoto, Japan), and are needed for the calculation of particle impact conditions. Powder morphologies were analyzed by scanning electron microscopy (SEM), using a Quanta 650 from FEI (Brno, Czech Republic) at an acceleration voltage of 20 kV.

The powder strengths were investigated by single particle compression tests following the routines developed by Assadi et al. (Ref 3, 10, 14, 20). The analyses were performed by using a modified microhardness testing device ZHU0.2 (Zwick Instruments, Germany). Single particles were individually compressed by applying a flat punch geometry under a rate of 0.1 mm/min until reaching a height reduction of minimum 50% for sufficient plastic deformation. In combination with the analysis routine established by Assadi et al. (Ref 10), the force–displacement data were developed into stress–strain diagrams for deriving particle yield strength (YS) and UTS. The powder strength data are needed for more precise calculation of

critical velocities and thus more realistic data on impact to critical velocity ratios η.

Calculation of Powder Impact Conditions

The calculations of particle impact conditions and critical velocities were performed by using the KSS software package from Kinetic Spray Solutions (Buchholz, Germany). The fluid dynamics calculations within this package are based on the models from Schmidt et al. (Ref 11) and Assadi et al. (Ref 12), and consider the respective cold spray parameter sets as well as feedstock powder data, including particle size distribution. For a more realistic description, the calculation of critical velocities considered the measured particle strengths as input data.

Cold Gas Spraying

The different cold spray experiments were performed with a commercial spray system of type 5/11 from Impact Innovations (Rattenkirchen, Germany). The spray system was used in combination with a water-cooled SiC nozzle of type OUT 1 (Impact Innovations, Rattenkirchen, Germany) with an expansion ratio of 5.6 and an expansion length of 160 mm. In the experiments, the powder was injected at a distance of − 128 mm upstream nozzle throat. Nitrogen was used as process and as carrier gas. All experiments were carried out at a fixed stand-off distance of 60 mm. For the deposition onto flat substrates to produce MFT samples, the gun traverse velocity was set to 250 mm/s covering a lateral area of 50 mm × 70 mm. The deposits were built-up to a thickness of around 3 mm. The cylindrical TCT test samples were coated by setting the kinematics to a traverse gun velocity of 4 mm/s and a sample rotation speed of 200 rpm, which corresponds to a circumference speed of 250 mm/s. The deposits for the TCT test samples were build-up in a thickness of around 1 mm. For ensuring good adhesion and minor efforts in surface preparation, $AlMg_3$ was selected as substrate material for both experiments. Substrate surfaces were cleaned with ethanol just before spraying. Details concerning process gas pressures and temperatures are given in Table 1.

Deposit Characterization

Deposit cross sections were prepared by the usual procedures (Ref 3, 27), here using OP-S (oxide polishing suspension, from Struers, Ballerup, Denmark) for the final polishing step. Deposit microstructures were investigated by optical microscopy (OM) using an instrument type VHX-7000 from Keyence (Osaka, Japan).

The cohesive strength of the produced material deposits was investigated by MFT as well as TCT tests. To guarantee sufficient statistical evidence, at least five samples per spray material and parameter setting were tested. The MFT as well as the TCT tests were performed using a universal testing machine of type Z100 from Zwick/Roell (Ulm, Germany).

For the preparation of MFT test samples, the deposit material was sprayed onto flat substrates and cut into desired test sample geometries (L*W*H: 30 × 5 × 0.5 mm; gauge length 9 mm) by electro-discharge erosion by setting the gauge direction and thus later the applied force orthogonal to the spray lines. Details of the specimen geometry (Fig. 1a) as well as an overview image of one of the Cu samples after testing (Fig. 1b) are shown in Fig. 1. In deviation to the standard for tensile testing, the experiments were performed using a load-controlled procedure with a fixed strain rate of 0.00025 1/s. The elongation was optically recorded by a CCD camera of type videoXtens and analyzed by the commercially available software testXpert, both from Zwick/Roell (Ulm, Germany).

Table 1 Applied process gas temperatures (T_{gas}), process gas pressures (p_{gas}) and calculated η values for mean particle sizes of 32 µm for Ti and 25 µm for Cu, respectively, as well as property data of the corresponding cold sprayed deposits (measured by MFT: strain to failure A_{MFT}, ultimate tensile strength UTS_{MFT}; measured by TCT: UTS_{TCT}; and porosity)

Condition	T_{gas}, °C	p_{gas}, MPa	η, d_{50}	A_{MFT}, %	UTS_{MFT}, MPa	UTS_{TCT}, MPa	Porosity, %
Titanium							
Low	700	5	0.86	0.2	279	160	7.0
Medium	850	5	0.96	0.2	326	212	1.5
High	1000	5	1.06	0.3	442	306	0.7
Copper							
Low	400	5	1.18	0.1	174	116	0.1
Medium	550	5	1.36	5.3	289	239	0.1
High	700	5	1.57	17.5	282	299	0.0

All experiments were performed using nitrogen as process gas, a cold spray system 5/11 and a nozzle type OUT 1 (both from Impact Innovations). An injection distance of − 128 mm was used in combination with a stand-off distance of 60 mm and a robot traverse (MFT tests)/sample circumferential (TCT tests) velocity of 250 mm/s

In order for producing the TCT samples, two rotation-symmetrical specimens (diameter: 24 mm; total length coated surface: 45 mm) were screwed onto a holder (Fig. 2a). The common shell of the two cylinders was then machined to obtain a notch free surface. The shell surface was then covered by a cold sprayed coating by applying a lathe during deposition, thereby assuring that rotational and traverse robot velocity match to the kinematic parameters that were used in coating flat samples for MFT testing. Afterward, the holder was removed, and the samples were tested by using a set-up similar to bond strength testing by using a load-controlled procedure with a testing speed of 1 mm/min (Fig. 2b). As given by samples geometries, the load in testing is applied perpendicular to the spray lines. Figure 2c displays the typical area of failure during a TCT test, whereas Fig. 2d shows a top view onto one of the two fracture surfaces, and thus onto the area that carried the load.

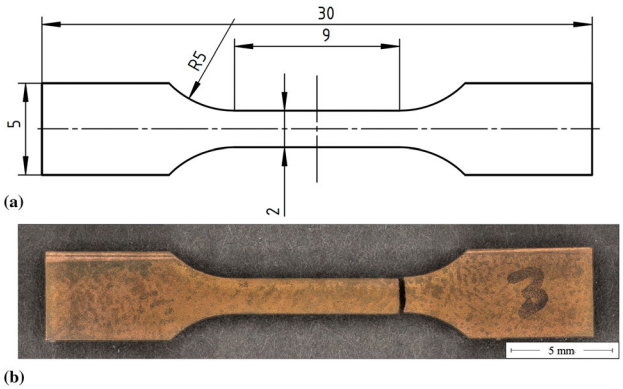

Fig. 1 Geometry of MFT test specimen: Sample geometry according to DIN EN ISO 6892–1 (a), and macro-view of one of the Cu samples after testing (b)

Selected fracture surfaces were investigated by scanning electron microscopy (SEM) using the secondary electron (SE) mode (Quanta 650, FEI, Brno, Czech Republic) to gain information about material deformation and fracture behavior.

Results

Powder Morphologies and Strengths

The morphologies of the Ti and the Cu powders as well as powder size distributions are shown in Fig. 3 Both powders have spherical shapes and show only few satellites or remaining fines (Fig. 3a, c). The results from laser scattering confirm a rather narrow particle size distribution of d_{10} = 22 µm, d_{50} = 32 µm and d_{90} = 49 µm for Ti and d_{10} = 18 µm, d_{50} = 25 µm and d_{90} = 35 µm for Cu powder, respectively (Fig. 3b, d).

Figure 4 summarizes the results of stress–strain measurements of individual particles of (Fig. 4a) Ti and (Fig. 4c) Cu as well as corresponding cross-sectional microstructures of the as received powders in (Fig. 4b) and (Fig. 4d). From the raw data, mean particle ultimate tensile strengths are derived and determined to 659 and 337 MPa for the Ti and the Cu powders, respectively, for both showing no obvious variation over particle sizes. For Ti, the data show some scatter. This could be attributed to either non-ideal spherical shape of some particles or non-isotropic plastic flow in case of inhomogeneous grain size distributions. The cross-sectional microstructures reveal that some Ti powder particles contain large grains that could contribute to anisotropic, single crystal like plastic flow.

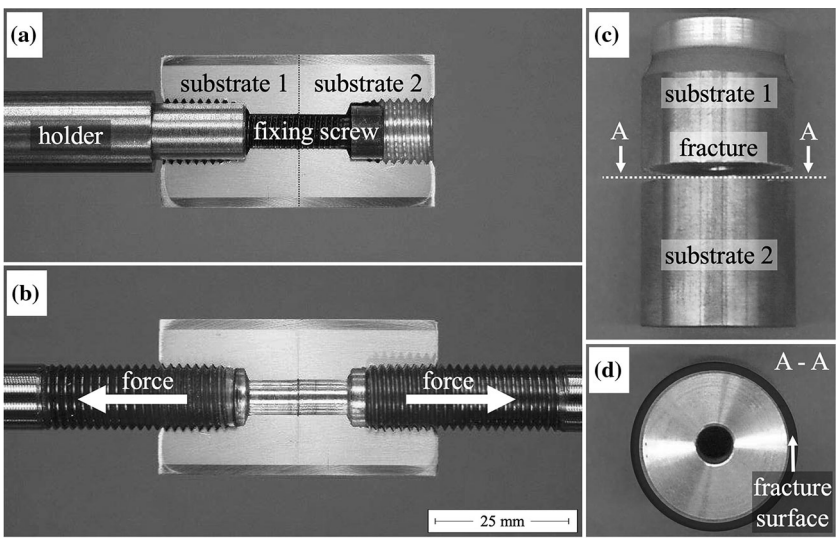

Fig. 2 Geometry of TCT test specimen: Longitudinal cut of the coated TCT sample screwed to the holder (a), longitudinal cut of the coated TCT sample ready for testing in a tensile machine (b), an example of the typical area of failure during testing (c), and top view onto one of the two fracture surfaces (d). Reprinted from T. Schmidt, F. Gärtner, and H. Kreye, New Developments in Cold Spray Based on Higher Gas and Particle Temperatures, Journal of Thermal Spray Technology, Vol. 15, pg. 488–494, Springer Nature (Ref 31)

Impact Conditions and Critical Velocities

Table 1 summarizes the applied cold spray conditions with respect to the used process gas temperatures (T_{gas}) and process gas pressures (p_{gas}) as well as respective η values calculated for the mean particle sizes of Ti (d_{50} = 32 µm) and Cu (d_{50} = 25 µm) powders. The parameter combinations were chosen to cover a broad range of η values, thus resulting in different deposit properties. Figure 5 shows the calculated particle impact conditions (compare Table 1) superimposed to the corresponding critical velocities, representing a window of deposition. For Ti (black triangles) as well as for Cu (gray circles), higher process gas temperatures lead to higher impact temperatures and higher impact velocities. The higher excess over critical velocities signifies higher η values, which within the range of selected spray parameters are increased from about 0.86 to 1.06 for cold gas spraying of Ti, and about 1.18 to 1.57 for Cu. The wide range of parameter sets should lead to significant changes in deposit properties and associated fracture behaviors.

Deposit Microstructures

Representative microstructures of the cold sprayed Ti as well as Cu deposits are given in Fig. 6 (a-c, g-i: overview; d-f, j-l: detail). The Ti deposit shown in Fig. 6a, d was processed with an η value of 0.86, which results in a high porosity of 7%. By increasing the parameter sets and thus η, the porosity can be reduced. Figure 6b, e show the microstructure of a Ti deposit sprayed at an η value of 0.96. The respective porosity was determined to 1.5%. Increasing η, in this case, to a value of 1.06, leads to a further reduction in the porosity of the deposited Ti down to 0.7% (Fig. 6c, f). The three Cu deposits displayed in Fig. 6g-i and Fig. 6j-l show almost no optical difference. The deposits were produced with relatively high η values of 1.18, 1.36, and 1.57, thus being quite homogeneous with very low porosities of 0.1, 0.1, and 0.0%, respectively.

Mechanical Deformation Behavior

For all parameter sets, the mechanical deposit properties were investigated by MFT tests. Examples of typical stress–strain diagrams of Ti and Cu deposits cold sprayed

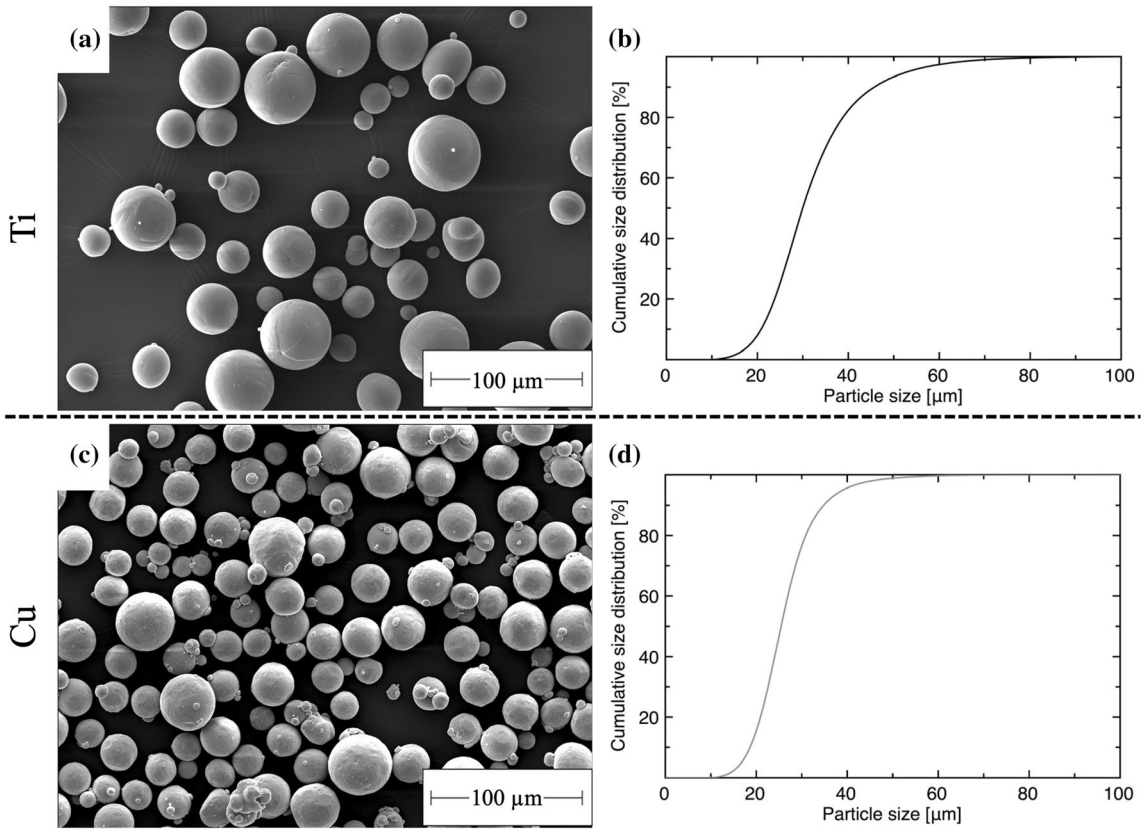

Fig. 3 Particle morphologies (SEM, SE-mode) of the (a) Ti and (c) Cu powder feedstock, and their corresponding cumulative size distributions (b), (d)

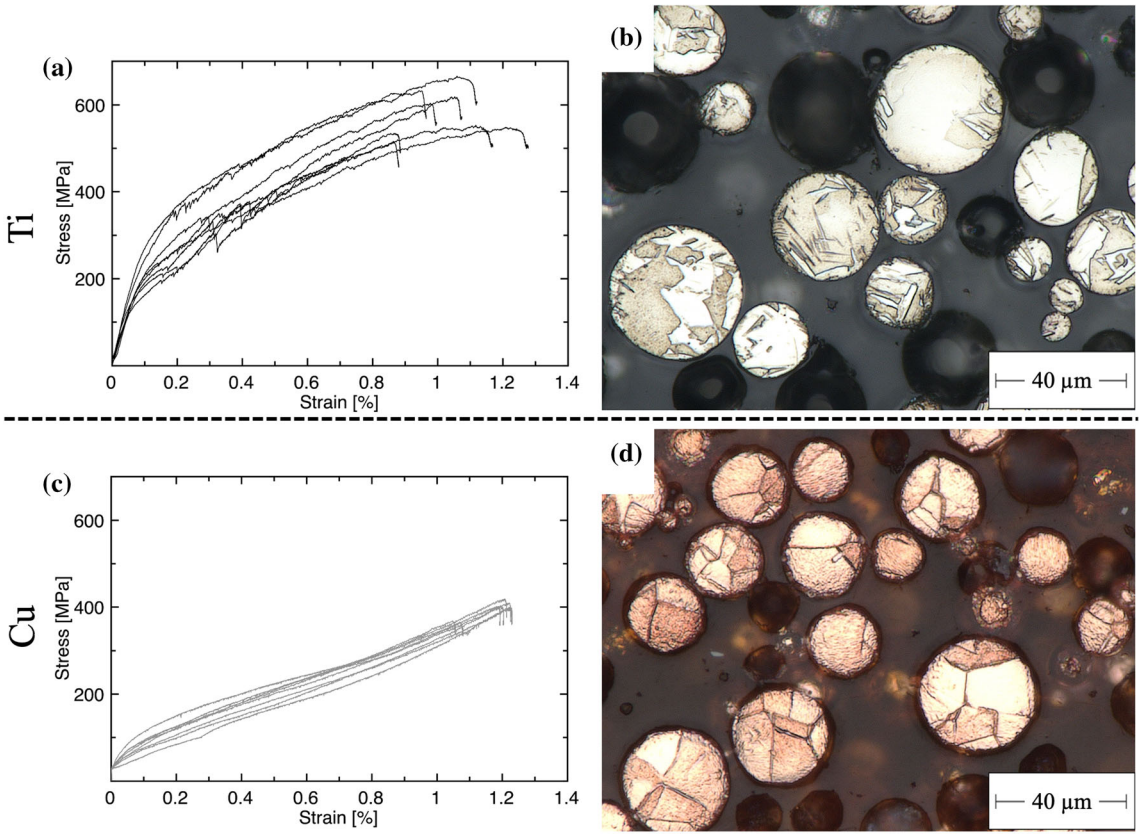

Fig. 4 Raw data of stress–strain curves as determined by particle compression tests as well as cross-sectional microstructures (optical microscopy) of the as received powders, (a, b) Ti and (c, d) Cu

with lowest, medium, and highest parameter sets within this comparison are shown in Fig. 7. For both materials, higher spray conditions (higher η values) lead to increased deposit strengths (UTS). However, an increased strength does not necessarily translate into a higher strain to failure. For the applied parameter sets, all Ti deposits (black curves) fail within the elastic regime. Also, the cold sprayed Cu deposit produced under the lowest process gas temperature and thus the lowest η value (solid gray curve) shows no plastic deformation and fails within the elastic regime. However, in contrast, the Cu deposit sprayed with a medium η value (dotted gray curve) already indicates plastic deformation reaching an elongation to failure of 5.3%. In the case of Cu, further enhancement of the process gas temperature (highest η value, dashed gray curve) then leads to a strain to failure of almost 18%. The significant differences between brittle and plastic failure of CS Cu deposits are also recognizable by comparing the two macro-images (insets at the sides of Fig. 7: left side: lowest η value, right side: highest η value) of the MFT samples after testing. The ductile sample already shows a reduction in cross-profile. The attained high plasticity can be attributed to thermal recrystallization occurring already during the deposition process (Ref 28).

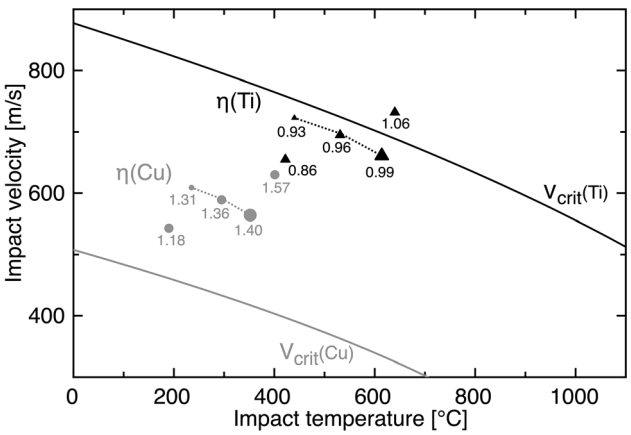

Fig. 5 Calculated particle impact conditions with respective η values of mean particle sizes (d50) for the applied parameter sets as well as critical velocities for the two used powders (black triangles: Ti and gray circles: Cu) as window of deposition. For the medium parameter sets, exemplary, the impact conditions are shown for d10, d50 and d90, corresponding to particle sizes of 22, 32 and 49 µm for Ti, and 18, 25 and 35 µm for Cu, respectively

Ultimate Tensile Strength Development

For comparison and correlation, tensile strength was also measured by TCT tests. Figure 8 shows the raw UTS data

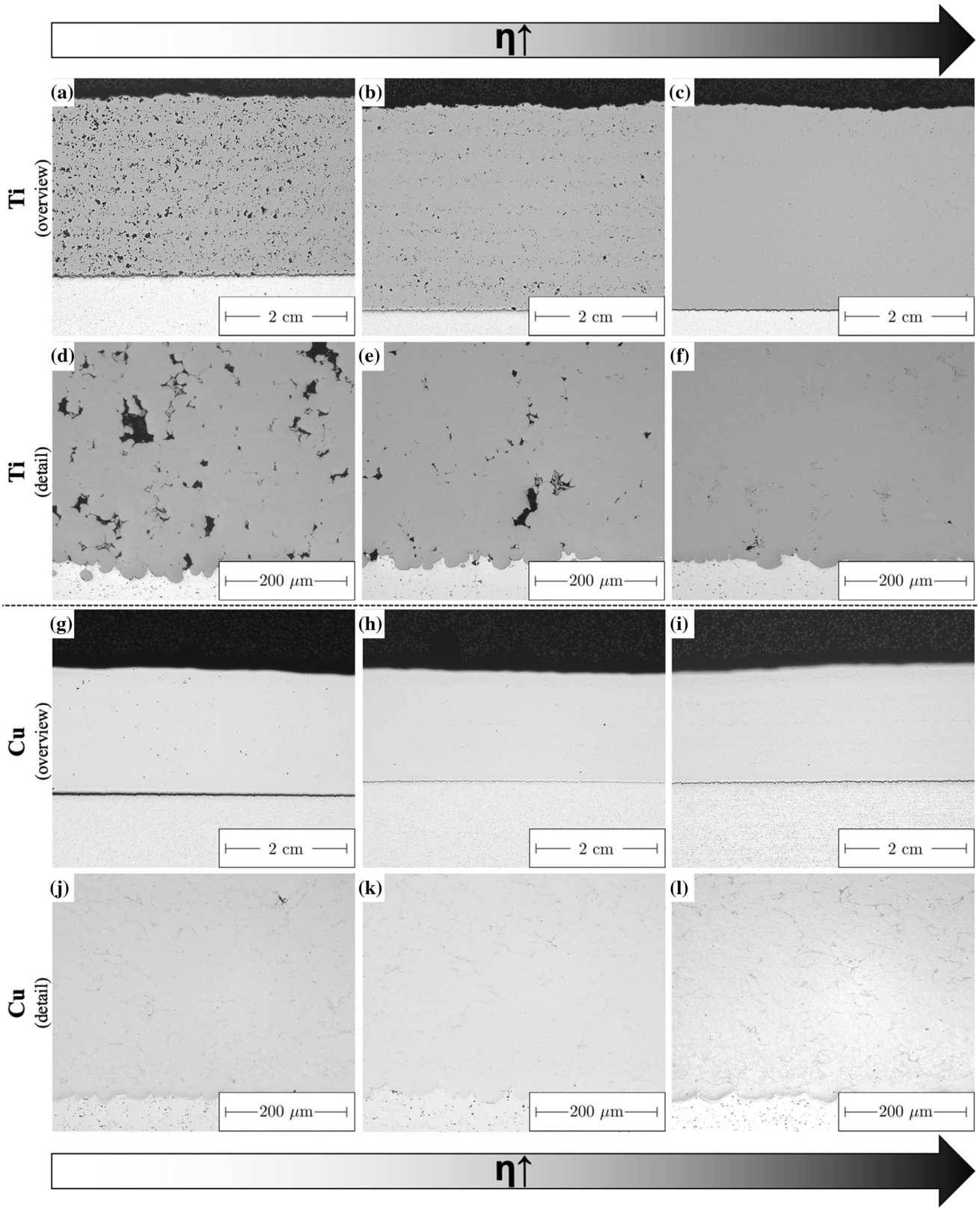

Fig. 6 Examples (a, b, c, g, h, i: overview; d, e, f, j, k, l: detail) of cross-sectional microstructures (optical microscopy) of cold sprayed deposits as obtained by applying individual η values of (a, d) 0.86, (b, e) 0.96, and (c, f) 1.06 in the case of Ti, as well as (g, j) 1.18, (h, k) 1.36, and (i, l) 1.57 for Cu

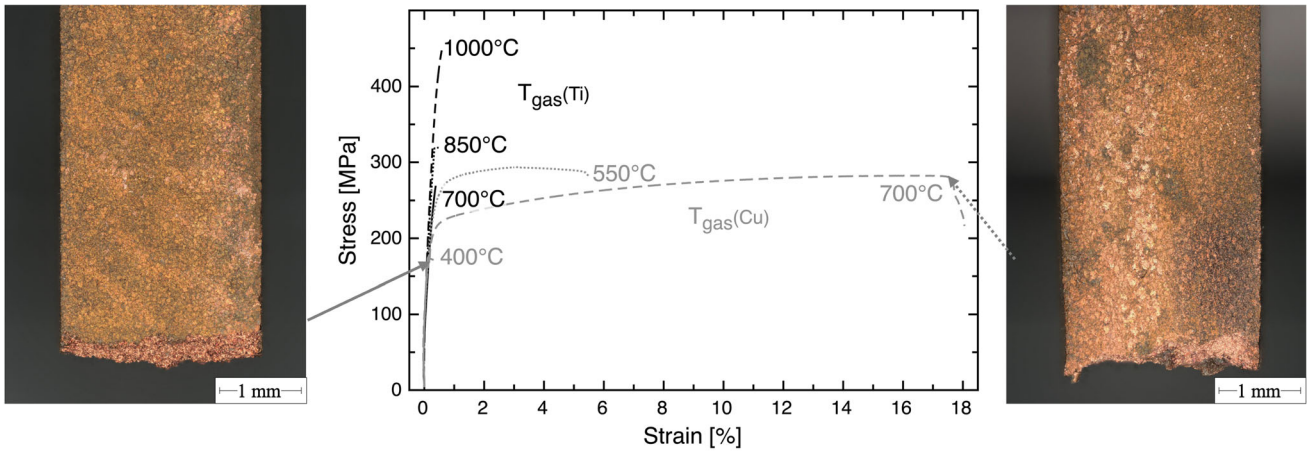

Fig. 7 Stress–strain curves of Ti (black) and Cu (gray) deposits recorded by MFT tests for lowest process gas temperatures/η values (solid line), medium process gas temperatures/η values (dotted line), and highest process gas temperatures/η values (dashed line), respectively. The inserts at the sides show macro-views of Cu MFT samples, produced with the lowest (left side) and highest (right side) η values, after fracture

from MFT (filled symbols) and TCT (empty symbols) tests, here without taking a notch factor into account, over η. The dashed/dotted lines are given as a guide for the eye for better visualization of the different dependencies within the linear regimes. Within the covered η regime from 0.86 up to 1.06, the strengths of the cold sprayed Ti deposits (black triangles) show an almost linear increase with η. Due to the more complex stress distribution, the tensile strengths measured by TCT tests are overall lower than those determined by MFT analyses. Both dependencies run with a similar slope, which is surprising under assuming a fixed notch factor. For the rather linear regime with η between 1.18 and 1.36, the above statements also apply to the MFT and TCT strength data of the cold sprayed Cu deposits (gray circles). However, the situation gets different for the Cu deposited at the highest η of 1.57. For such high η values, the strength seems to run into a saturation limit reaching bulk-like properties and even allowing for possible decrease by reduced work hardening effects. In parallel, the differences between MFT and TCT data appear to diminish. The obtained saturation limit or even decrease in UTS can be attributed to superimposed material softening by already occurring recovery and recrystallization effects during material deposition. The diminishing difference between MFT and TCT strengths can be explained by changes of stress states and stress reduction at the two substrate faces acting as a notch in the case of the TCT tests. Thus, the gained (local) plasticity due to higher spray parameter sets proves a stronger influence on deposit strengths as obtained by TCT testing than for the MFT tests. The increased material ductility helps to compensate for introduced stress concentrations during testing, which are higher for the TCT specimen than for MFT specimen.

For exploring the unexpected slopes and differences of strength data for increasing η values by means of a notch factor, Fig. 9 provides a direct correlation between the raw UTS data as gained by MFT and TCT tests for Ti (black triangles) and Cu (gray circles), respectively. It may be noted here that the attained differences in absolute strengths are due to individual properties of Ti or Cu in highly work-hardened states. The dotted line in this correlation corresponds to the assumption of a fixed notch factor of 1.6, according to the literature that describes the stress concentration during TCT testing (Ref 24, 26, 27). The comparison of the measured data indicates significant differences in individual notch factors. Particularly for higher strength data, deviations to lower values are observed. This behavior could possibly be attributed to changes in the deformation behavior as discussed in more detail in the following paragraph.

Fracture Morphologies

The observed ranges of elongation correspond to differences in local deformation features and fracture morphologies of the deposits. Figure 10 shows examples of fracture surfaces after MFT and TCT testing of Ti deposits taken from the middle of the samples that reached A* = 0.2%, processed with η = 0.86 (Fig. 10a, d), A* = 0.2%, processed with η = 0.96 (Fig. 10b, e) and A* = 0.3%, processed with η = 1.06 (Fig. 10c, f). The rise in impact conditions for the Ti deposited with an η above 1.00 causes a significant increase in particle deformation. In addition, bonded areas show significant amounts (> about 30%) of ductile dimple fracture, despite the small differences concerning the achieved strain to failure. In

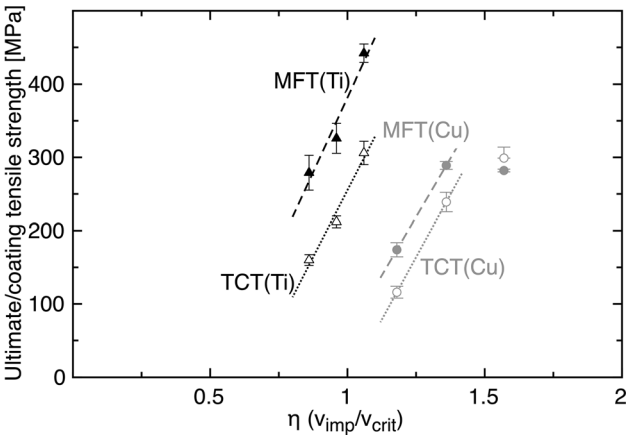

Fig. 8 Tensile strengths, obtained by MFT tests (filled symbols) and by TCT tests (empty symbols) for the cold sprayed Ti (black triangles) and Cu deposits (gray circles) plotted against η. The dashed/dotted lines are given as a guide for the eye to visualize the different dependencies between MFT and TCT tests for the two different spray materials

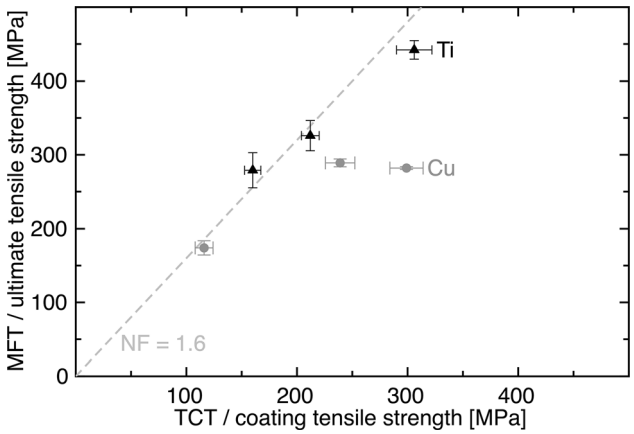

Fig. 9 Correlation between ultimate tensile strengths, gained by MFT tests and coating tensile strengths, gained by TCT tests for Ti (black triangles) and Cu (gray circles). Respective notch factors can be calculated as the ratios between individual UTS_{mft} and UTS_{tct} data. The dashed line represents the correlation for assuming a fixed notch factor of 1.6

contrast, at the two lower impact conditions, nearly the whole surface shows plain fracture at non-bonded interfaces of less deformed particles (i), as well as lower amounts of the small-scaled dimple sites (ii) on the fracture surface, as visible in Fig. 10a, b and in Fig. 10d, e. For the higher impact condition, splats are more deformed and show higher amounts of metallurgically bonded regimes. This is demonstrated by significant amounts of dimples here occurring in wide size ranges (iii). Nevertheless, main failure is still attributed to crack growth starting from poorly bonded interfaces (iv) as given in Fig. 10c and f. Based on the fracture morphologies, no obvious difference between failure in MFT and TCT tests can be derived. The slightly lower degree in particle deformation in case of the TCT example shown in Fig. 10d might be attributed to the local selection of feature details during microscopy.

Figure 11 displays selected fracture surfaces after MFT and TCT testing of Cu deposits that reached A* = 0.1%, sprayed with η = 1.18 (Fig. 11a, d), and A* = 5.3%, sprayed with η = 1.36 (Fig. 11b, e), and A* = 17.5%, sprayed with η = 1.57 (Fig. 11c, f). In the case of the lower spray condition and deposits reaching low strain to failure (Fig. 11a, d), the fracture surfaces are dominated by smooth, predominantly brittle inter-splat failure (I) and only show minor traces of ductile deformation during rupture. However, the deposit splats are highly deformed (II) and to a certain degree already show failure under plastic deformation during testing (III). Thus, planar features do not only indicate inter- (I), but to some extent also brittle transparticle failure (IV). If occurring, the latter is mainly due to high degrees of splat work hardening during the deposition in combination with already sufficient amounts of well-bonded particle–particle interfaces. By the combination of these features, the crack growth paths, as denoted by (I), follow mainly along the particle–particle interfaces by microcrack growth and bridge into neighboring non-bonded interfaces or partially divert to transparticle or trans-splat failure. For the high parameter set and obtained high strain to failure (Fig. 11c, f), the fracture surfaces are dominated (> 90%) by rather uniform ductile features, mostly spreading through the splat interior. However, as seen in the micrograph, the dimple-like plastic deformation patterns (V) still scale to splat dimensions. For the medium impact condition, the observed fracture morphology shown in Fig. 11b, e shows similar basic features as already described for the lowest and highest parameter set. Judging from the micrograph, about 70–80% of the fracture surface is showing ductile features.

As for the CS Ti deposits, the described features under one spray parameter set are also similar for the MFT and TCT test samples of the CS Cu. This proves that observed differences in crack propagation and deposit performance are given by internal microstructural details and reduced work hardening effects allowing for plasticity, rather than by macroscopic phenomena.

Discussion

The results confirm the clear improvement of deposit strengths with increasing impact conditions and respective η values. Foremostly, this is governed by the overall amounts of well-bonded interfaces. Respectively, fracture surface patterns increasingly show features by ductile fracture. However, at least for copper, deviations in strength trends are observed for impact conditions that

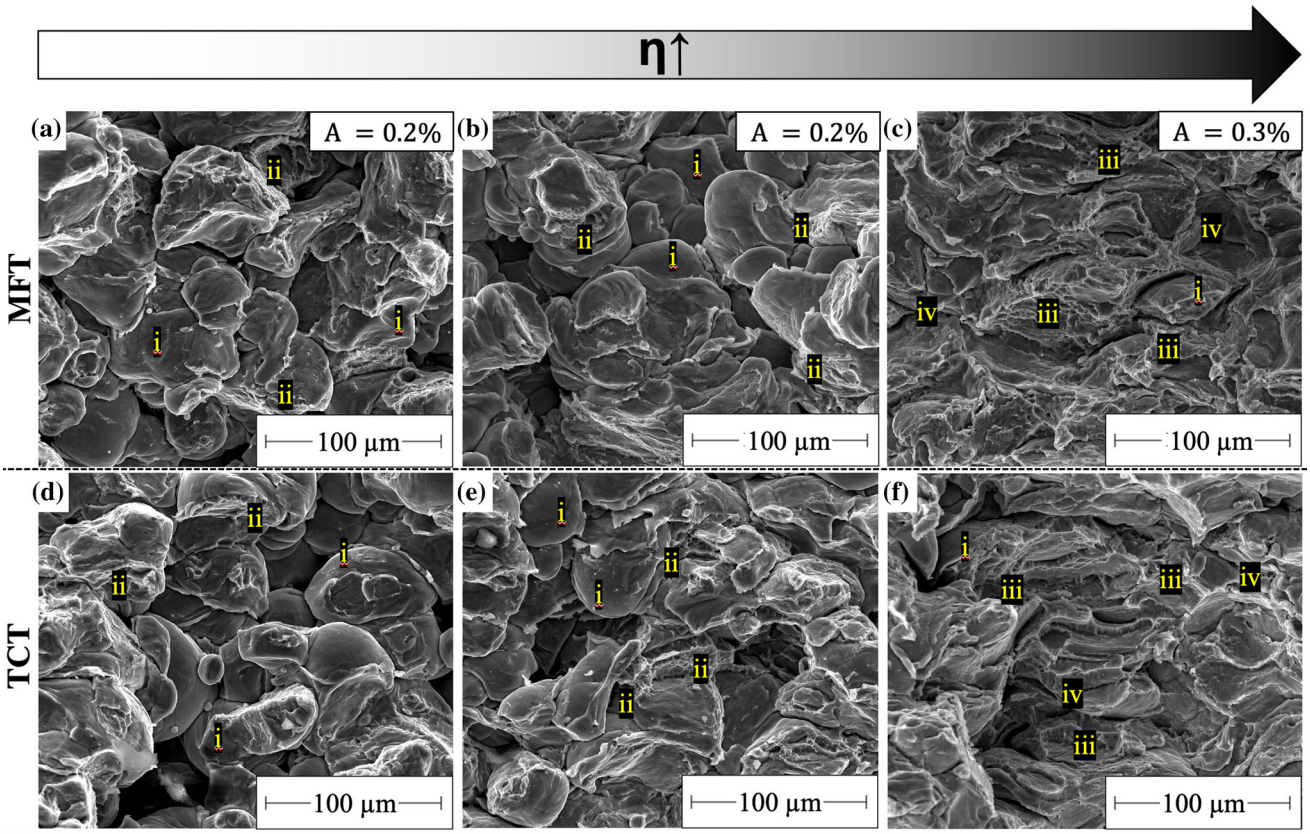

Fig. 10 SEM close-up micrographs of fracture surfaces of Ti deposits after MFT (a, b, c) and after TCT (d, e, f) testing for different deposit qualities processed with η values of (a, d) 0.86, (b, e) 0.96, and (c, f) 1.06. The obtained elongations to fracture are given as inserts (a, b, c). The markers show, i: less deformed particles, ii: small dimples by ASI, iii: plastic deformation and dimple failure at well-bonded areas, and iv: crack growth at poorly bonded interfaces

ensure more ductile deformation at higher η values. To some extent, these trends are confirmed by respective fracture surfaces.

In the case of Cu deposits, the stress diagrams given in Fig. 7 already give some hints on possible reasons. Rising the eta from 1.47 to 1.57 increases the strain to failure, but decreases the yield strengths (YS) and the ultimate tensile strengths (UTS), rather similar to annealing effects causing recovery and recrystallization of cold worked Cu or high-quality CS deposits obtained by using He as propellant gas (Ref 6). Similarly, the increase in elongation to fracture and decrease in strengths (YS and UTS) of Cu deposited by higher process gas temperatures during CS with N_2 can be attributed to annealing and recrystallization effects caused by the attained temperatures of the deposit surface under the spray spot. Apart from these macroscopic issues, possible stress concentrations and notch factors are additionally influenced by micro-scale annealing effects and thus very localized plasticity, not necessarily depending on overall enhanced surface temperatures.

For developing a more quantitative description, the following paragraphs supply more details on influences of stress concentrations on the deformation behavior.

Influences of Deposit Plasticity on Stress Concentration and Notch Factors

The results demonstrate that the effects of possible stress concentrations on fracture in TCT testing depend on deposit qualities as attained under respective spray conditions. Therefore, a uniform description by a fixed notch factor is not appropriate for comparison with uniaxial loading in MFT analyses. For gaining more insights into the role of associated plasticity, the individual notch factors of cold sprayed deposits of the two investigated materials are plotted in Fig. 12 against the strain to failure attained by MFT testing (Ti: black triangles Cu: gray circles). The dotted lines are just given as a guide for the eye to indicate different slopes and dependencies. The comparison shows that attained notch factors decrease with increasing strain to failure. Furthermore, in Fig. 12, the rates of decrease appear to be high at low, and low at high strain to failure, respectively. It may be argued that the transition should also somehow depend on intrinsic material's deformability or toughness. However, due to work hardening, differences in bulk strain to failure are only to minor extent reflected by the material's properties and rather governed by local

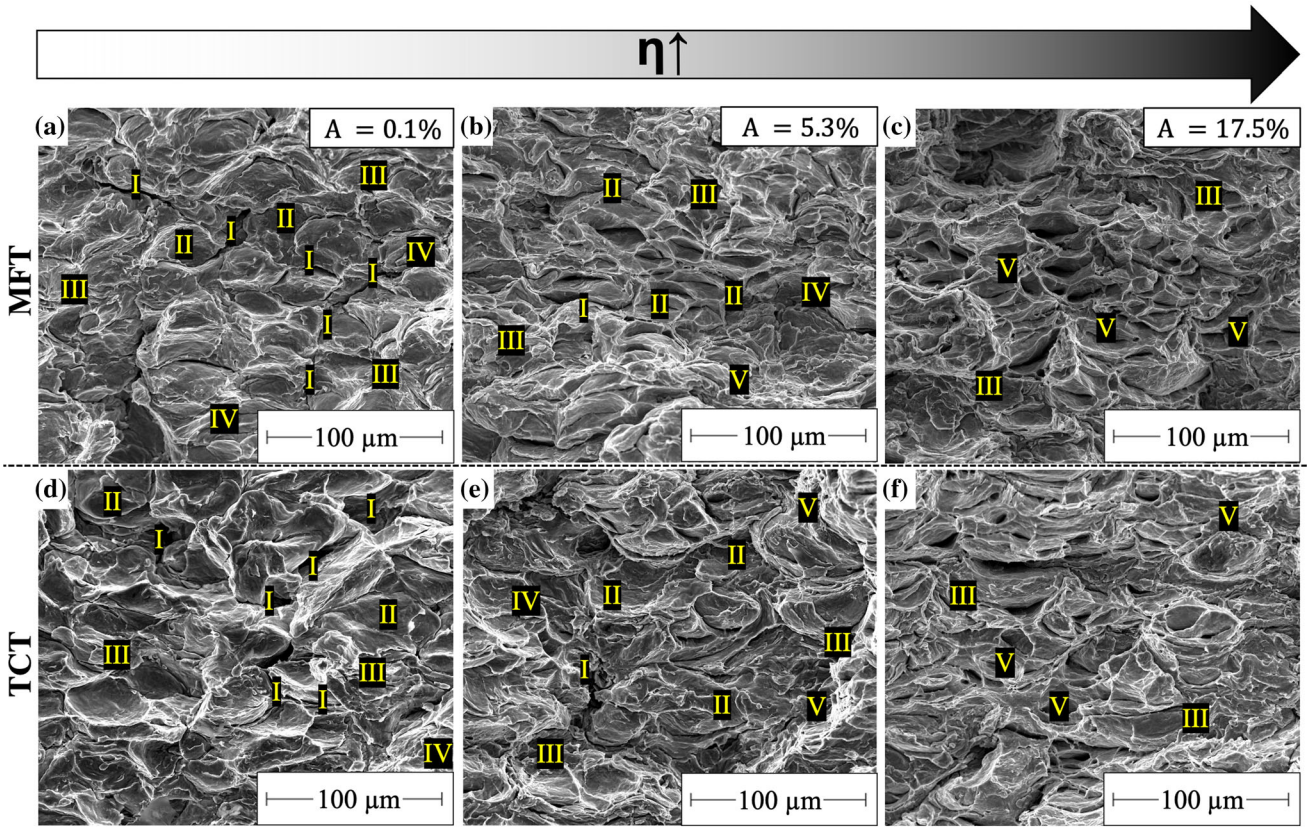

Fig. 11 SEM close-up micrographs of fracture surfaces of Cu deposits after MFT (a, b, c) and TCT (d, e, f) testing for different deposit qualities processed with η values of (a, d) 1.18, (b, e) 1.36, and (c, f) 1.57. The obtained elongations to fracture are given as inserts (a, b, c). The markers denote, I: crack growth at non-bonded interfaces, II: highly deformed areas showing no ASI, III: highly deformed areas showing plastic deformation, IV: brittle trans-splat failure, and V: ductile dimple failure

plasticity and the fraction of bonded interfaces. Thus, after cold spraying, the local deposit features and properties are highly dependent on the used spray parameter sets. At low strain to failure, the deposit is presumably rather brittle by high strain hardening or contains large fractions of unbonded interface area with overcritical crack length. Both would correspond to the rather low η regime. At higher η values, the fraction of bonded interface area increases until cracks are subcritical for fast failure. In addition, more (excess) heat is produced then, leading to local recrystallization, and thus to restoring some ductility. Ductility will slow down macroscopic crack growth by crack blunting, further contributing to a decrease in notch factor. In the case of high-quality cold sprayed Cu, even a notch factor of about unity is reached for the strain to failure exceeding 15%. A notch factor of unity basically indicates defect-free bulk behavior. In the present case, defects are still to be expected, but are subcritical for crack initiation and growth, presumably due to a very high fraction of bonded interface area and significant local ductility by recrystallization phenomena. The rate of decrease in notch factor may indeed be material-dependent. However, it is also conceivable that initial reduction in unbonded interface fraction can generally lead to a faster decrease in the notch factor, when the material is still almost ultimately strain hardened and brittle. Recrystallization phenomena pick up after reaching saturation in bonded interface area and then only lead to a lower slope ultimately toward bulk behavior. The change of trend could also possibly be associated with length scales of associated plastic deformation to reduce local stress states. Keeping in mind that the microstructures are rather inhomogeneous, as derivable from the fracture morphologies, high strain to failure, as here prominently obtained for the higher quality range of the Cu deposits, involves plastic deformation on a macro-scale, covering several well-bonded and deformable spray splats and length scales of some tens of microns. At low strain to failure, any plasticity remains limited within a micro-regime and does not involve deformation of bonded splat ensembles, here being more prominent for the lower quality range of the Ti deposits. In detail, even micro-scale deformation could reduce stress concentration as schematically illustrated in Fig. 13 for an initial crack within materials of slightly different ductility. As sketched

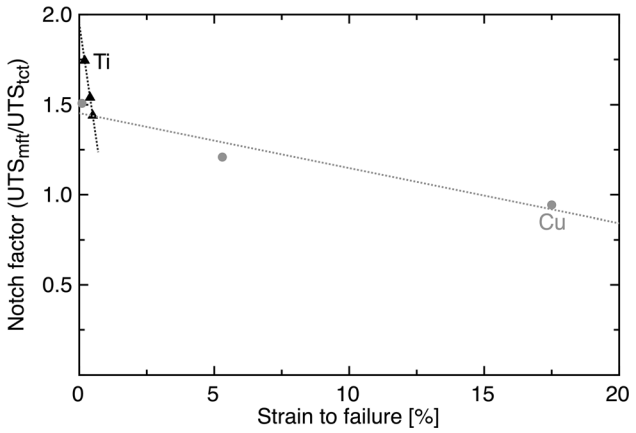

Fig. 12 Calculated individual correlation factors as function of the strain to failure as gained by MFT tests for the different Ti (black triangles) and Cu (gray circles) deposits. The dotted lines are given as a guide for the eye to emphasize different slopes

in Fig. 13a for a rather brittle material with low strain to failure and ductility, the local stress concentration at the tip of an internal crack could exceed strength limits (highlighted by red mark) and lead to crack growth and early fracture. This situation would result in geometrically determined stress concentrations and thus a high notch factor. The situation for a material with slightly higher strain to failure is sketched in Fig. 13b. Even few local plasticity (highlighted by green mark) could reduce local stresses and allow for a slightly increased crack tip radius. Stress states below local deposit strength does not necessarily result in crack growth. For this situation, consequences by geometrically caused stress concentrations already have less influence on crack growth, thus leading to a lower notch factor.

In reality, the effects by local stress concentrations and deformation are rather complex and depend on stress states related to external geometries, microscopic crack lengths and crack radii as well as on micro- and macro-features that are obtained by the deformation under particle impact and determine material ductility and toughness in the vicinity of bonded and non-bonded interfaces. Cold sprayed deposits usually exhibit significantly different microstructures in the interface area as compared to the interior of splats. In addition, even at zero porosity, deposits are full of microcracks, and only the well-bonded interface areas carry external loads. Whether cracks can grow or not depends on local stress concentration and the deformation of the whole ensemble in the surrounding. In this way, crack growth or material failure gets a matter of local and global toughness. The toughness in the vicinity of bonded areas is then determined by the local microstructures. For example, areas of dynamic recrystallization on micron or sub-micron scale should provide a better deformability than obtained in the highly strain hardened environment (Ref 3, 7). Actual research under this ongoing project combines investigations by micro-deformation and modeling in order to reveal more details about this complex interplay. Nevertheless, the decreasing influence of stress concentrations under increased plasticity already provides some hints on fracture behavior and possible influences on deposit toughness. We expect that deposit quality-dependent ranges for associated material deformation continuously increase from micro- to macro-scale. However, for practical aspects, the present results already demonstrate the influence of plasticity and strain to failure on correlations between the types of tensile testing methods and thus the notch factor needed for analyses by TCT tests.

Influence of Spray Parameter Sets on attainable Notch Factors

So far, the concept of η as ratio between critical and impact velocities has been successfully used to describe influences of powder strength and spray conditions on deposit properties (Ref 12, 14, 21, 30). However, here the main focus was given to explore direct correlations to ultimate deposit tensile strengths. Possible forecasts on ductility by η are less straightforward as shown in Fig. 14 for the example of strain to failure. The attained strain to failure increases with η, but does not allow for deriving a simple correlation, due to significant different slopes for the two materials particularly for η around unity. Another attempt can be made by a suitable correlation between the results from MFT and TCT testing. Respective data are shown in Fig. 15 in terms of calculated notch factors for TCT testing and corresponding η values covering the quality ranges of investigated Ti and Cu deposits. The notch factor shows a linear decrease with increasing η ratios, as shown by the dashed line, and can be described by one uniform fitting function for Ti and Cu as deposit materials and the different quality ranges:

$$NF = 2.60 - 1.03 \times \eta \quad \text{(Eq 4)}$$

This indicates that the notch factor for the description of stress concentration in TCT analyses within a certain validity range could supply a universal description of present ductility and possible local stress releases. The validity range is defined by limitations of possible stress concentrations to 1.7 considering maximum crack lengths and orientations at low η values and to 1.0 at high η values greater 1.5 assuming negligible influence by stress concentration under sufficient plasticity. If applicable to other deposit materials, such uniform correlation would allow an easy forecast for required spray conditions to adjust deposit toughness.

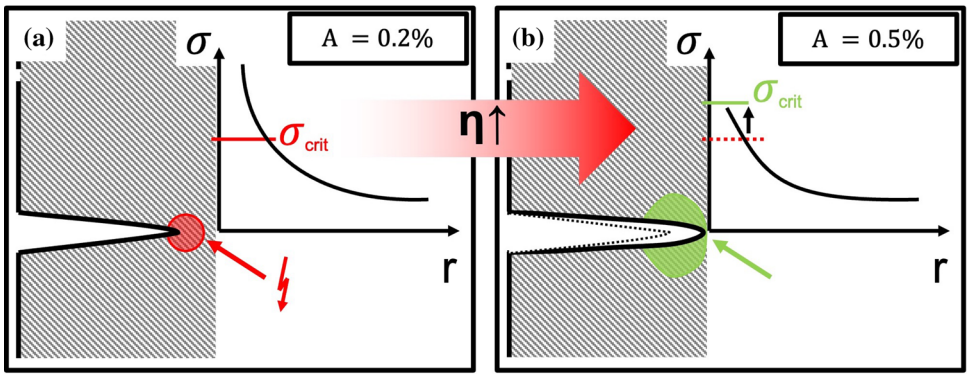

Fig. 13 Schematics for possible crack growth in (a) predominantly brittle and (b) slightly ductilized deposits. As possibly observed in cold sprayed Ti, where (a) describes a case deposited with rather low η values where stress concentration at the tip of an internal crack exceeds limits for growth and leads to early fracture and (b) considers a deposit processed at slightly higher η values in which local plastic deformation reduces present stress concentrations and together with increased crack tip radius enables for higher limits for crack growth

Summary and Conclusion

This study demonstrates a first attempt and approach to assess resistance against crack nucleation and growth based on local microstructural features in cold spray deposits. Based on experimental data and different approaches for tensile testing of cold sprayed deposits, the present study provides a new concept for deriving information on local toughness and required scaling factors for data evaluation obtained by applying different mechanical testing methods. The use of micro-flat tensile (MFT) and tubular coating tensile (TCT) tests for cold sprayed Ti and Cu deposits of different quality ranges by tuned parameter sets allows to derive quantitative data on individual strengths, strain to failure and possible correlations in terms of the notch factor between MFT and TCT tests. The overall assessment is supported by microstructural investigations and fracture surface analyses. The following points summarize the major conclusions:

- Deposit strengths and elongations to failure scale with parameter sets for cold spray deposition.
- An increased elongation to failure is associated with larger fractions of well-bonded interface area as well as higher ductility in the vicinity of cracks.
- Even macroscopically restricted deformability could be associated with local micro-scale plasticity leading to a release of geometrically induced stress concentrations and to crack blunting.
- The correlation, usually defined as notch factor between individual MFT and TCT test data, decreases toward unity with increasing ductility and elongation to failure.
- In using TCT tests for deposit analyses, care should be taken regarding applicable notch factors. Instead of a fixed constant notch factor, individual notch factors related to the quality of the deposit should be used for estimating strengths. Respective deposit qualities may

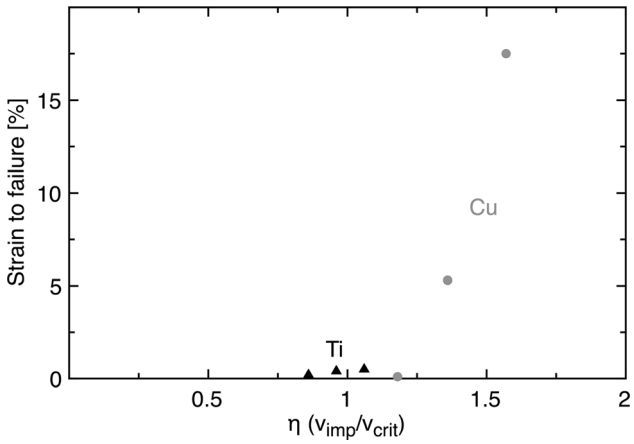

Fig. 14 Correlation between individual η ratios for the different quality ranges of Ti and Cu deposit build-up and strain to failure measured by MFT tests

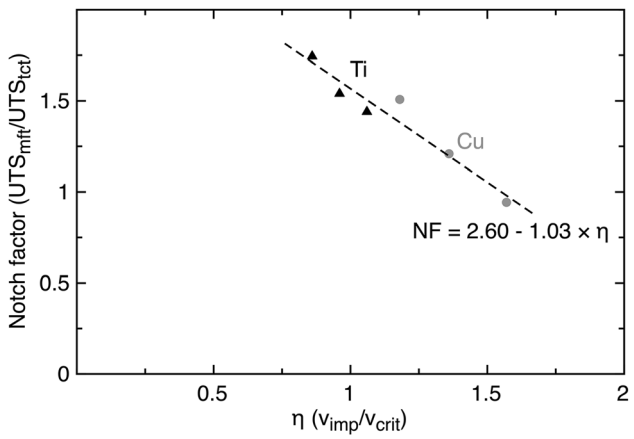

Fig. 15 Correlation between individual η ratios for the different quality ranges of Ti and Cu deposit build-up and calculated correlation factors. The dashed line in corresponds to the linear correlation between the notch factor and η, covering the deposit quality ranges of both materials

be reflected in terms of η as ratio between particle impact velocity and critical velocity.

A more accurate description and generalization of the new concept in this study, i.e., to use the notch factor as a function of η for a description of local deformability and stress concentration sensitivity, is ongoing work and will require more experiments and data, covering also several different materials. This concept then aims to contribute to a better understanding of crack growth in cold sprayed deposits and may also allow to predict critical failure conditions.

Acknowledgements The authors acknowledge the financial support of the German Research Foundation (DFG)—project number 448318292. The authors also like to thank in alphabetical order Thomas Breckwoldt, Camilla Schulze, and Marion Kollmeier for technical support during this study. We also thank all other HSU materials technology team members for fruitful discussion on the topic.

Funding Open Access funding enabled and organized by Projekt DEAL.

References

1. W. Li, C. Cao and S. Yin, Solid-state cold spraying of Ti and Its Alloys: A Literature Review, *Prog. Mater Sci.*, 2020, **110**, 100633.
2. F. Gärtner, T. Schmidt, T. Stoltenhoff and H. Kreye, Recent Developments and Potential Applications of Cold Spraying, *Adv. Eng. Mater.*, 2010, **8**(7), p 611-618.
3. C. Huang, M. Arseenko, L. Zhao, Y. Xie, A. Elsenberg, W. Li, F. Gärtner, A. Simar and T. Klassen, Property Prediction and Crack Growth Behavior in Cold Sprayed Cu Deposits, *Mater. Des.*, 2021, **206**, 109826.
4. K. Bobzin, W. Wietheger, J. Hebing and L. Gerdt, Softening Behavior of Cold-Sprayed Aluminum-Based Coatings AA1200 and AA7075 During Annealing, *J. Therm. Spray Technol.*, 2020, **30**, p 358-370.
5. H. Koivuluoto, J. Larjo, D. Marini, G. Pulci and F. Marra, Cold-Sprayed Al6061 Coatings: Online Spray Monitoring and Influence of Process Parameters on Coating Properties, *Coatings*, 2020, **10**, p 348.
6. F. Gärtner, T. Stoltenhoff, J. Voyer, H. Kreye, S. Riekehr and M. Koçak, Mechanical Properties of Cold-Sprayed and Thermally Sprayed Copper Coatings, *Surf. Coat. Technol.*, 2006, **200**(24), p 6770-6782.
7. C. Borchers, F. Gärtner, T. Stoltenhoff, H. Assadi and H. Kreye, Microstructural and Macroscopic Properties of Cold Sprayed Copper Coatings, *J. Appl. Phys.*, 2003, **93**, p 10064-10070.
8. M.V. Vidaller, A. List, F. Gärtner, T. Klassen, S. Dosta and J.M. Guilemany, Single Impact Bonding of Cold Sprayed Ti-6Al-4V Powders on Different Substrates, *J. Therm. Spray Technol.*, 2015, **24**, p 644–658.
9. T. Schmidt, F. Gärtner, H. Assadi and H. Kreye, Development of a Generalized Parameter Window for Cold Spray Deposition, *Acta Mater.*, 2006, **54**, p 729-742.
10. H. Assadi and F. Gärtner, Particle Compression Test: A Key Step towards Tailoring of Feedstock Powder for Cold Spraying, *Coatings*, 2020, **10**(5), p 458
11. T. Schmidt, H. Assadi, F. Gärtner, H. Richter, T. Stoltenhoff, H. Kreye and T. Klassen, From Particle Acceleration to Impact and Bonding in Cold Spraying, *J. Therm. Spray Technol.*, 2009, **18**(5-6), p 794-808.
12. H. Assadi, T. Schmidt, H. Richter, J.O. Kliemann, K. Binder, F. Gärtner, T. Klassen and H. Kreye, On Parameter Selection in Cold Spraying, *J. Therm. Spray Technol.*, 2011, **20**(6), p 1161-1176.
13. H. Assadi, F. Gärtner, T. Stoltenhoff and H. Kreye, Bonding Mechanism in Cold Gas Spraying, *Acta Mater.*, 2003, **51**(15), p 4379-4394.
14. C. Huang, A. List, J. Shen, B. Fu, S. Yin, T. Chen, B. Klusemann, F. Gärtner and T. Klassen, Tailoring Powder Strengths for Enhanced Quality of Cold Sprayed Al6061 Deposits, *Mater. Des.*, 2022, **215**, 110494.
15. H. Assadi, F. Gärtner, T. Klassen and H. Kreye, Comment on "Adiabatic Shear Instability is not Necessary for Adhesion in Cold Spray," *Scripta Mater.*, 2019, **162**, p 512-513.
16. A. List, C. Lyphout, M. Villa, F. Gärtner, and T. Klassen, Mechanical Properties of Cold-Sprayed Ti6Al4V Coatings, *Thermal Spray 2013: Proceedings of the International Thermal Spray Conference*, May 13-15, 2013 (Busan, South Korea), ASM International, p 155-160
17. M. Hassani-Gangaraj, D. Veysset, V.K. Champagne, K.A. Nelson and C.A. Schuh, Adiabatic Shear Instability is not Necessary for Adhesion in Cold Spray, *Acta Mater.*, 2018, **158**, p 430-439.
18. M. Hassani-Gangaraj, D. Veysset, V.K. Champagne, K.A. Nelson and C.A. Schuh, Response to Comment on "Adiabatic Shear Instability is not Necessary for Adhesion in Cold Spray," *Scripta Mater.*, 2019, **162**, p 515-519.
19. M.A. Adaan-Nyiak and A.A. Tiamiyu, Recent Advances on Bonding Mechanism in Cold Spray Process: A Review of Single-Particle Impact Methods, *J. Mater. Res.*, 2023, **38**, p 69-95.
20. H. Assadi, I. Irkhin, H. Gutzmann, F. Gärtner, M. Schulze, M. Villa Vidaller and T. Klassen, Determination of Plastic Constitutive Properties of Microparticles Through Single Particle Compression, *Adv. Powder Technol.*, 2015, **26**(6), p 1544-1554.
21. S. Krebs, F. Gärtner and T. Klassen, Cold Spraying of Cu-Al-Bronze for Cavitation Protection in Marine Environments, *J. Therm. Spray Technol.*, 2015, **24**(1-2), p 126-135.
22. R.C. Dykhuizen and M.F. Smith, Gas Dynamic Principles of Cold Spray, *J. Therm. Spray Technol.*, 1998, **7**(2), p 205-212.
23. D.L. Gilmore, R.C. Dykhuizen, R.A. Neiser, T.J. Roemer and M.F. Smith, Particle Velocity and Deposition Efficiency in the

Cold Spray Process, *J. Therm. Spray Technol.*, 1999, **8**(4), p 576-582.
24. C.-P. Gieseler, "Correlations for Strength Determination by MFT- and TCT-Tests", Helmut-Schmidt-University - University of the Federal Armed Forces Hamburg, Master Thesis, 2020.
25. C. Huang, A. List, L. Wiehler, M. Schulze, F. Gärtner and T. Klassen, Cold Spray Deposition of Graded Al-SiC Composites, *Addit. Manuf.*, 2022, **59**, 103116.
26. T. Schmidt, F. Gärtner and H. Kreye, *Tubular-Coating-Tensile-Test*, Helmut-Schmidt-University - University of the Federal Armed Forces Hamburg, Data Sheet, 2008.
27. K. Binder, J. Gottschalk, M. Kollenda, F. Gärtner and T. Klassen, Influence of Impact Angle and Gas Temperature on Mechanical Properties of Titanium Cold Spray Deposits, *J. Therm. Spray Technol.*, 2011, **20**(1-2), p 232-242.
28. R. Singh, J. Kondás, C. Bauer, J. Cizek, J. Medricky, S. Csaki, J. Čupera, R. Procházka, D. Melzer and P. Konopík, Bulk-Like Ductility of Cold Spray Additively Manufactured Copper in the As-Sprayed State, *Additive Manufacturing Letters*, 2022, **3**, 100052.
29. C. Chen, Y. Xie, S. Yin, W. Li, X. Luo, X. Xie, R. Zhao, C. Deng, J. Wang, H. Liao, M. Liu and Z. Ren, Ductile and High Strength Cu Fabricated by Solid-State Cold Spray Additive Manufacturing, *J. Mater. Sci. Technol.*, 2023, **134**, p 234-243.
30. S. Bagherifard, J. Kondas, S. Monti, J. Cizek, F. Perego, O. Kovarik, F. Lukac, F. Gärtner and M. Guagliano, Tailoring Cold Spray Additive Manufacturing of Steel 316 L for Static and Cyclic Load-Bearing Applications, *Mater. Des.*, 2021, **203**, 109575.
31. T. Schmidt, F. Gärtner and H. Kreye, New Developments in Cold Spray Based on Higher Gas and Particle Temperatures, *J. Therm. Spray Technol.*, 2006, **15**(4), p 488-494.